

RealRep: Generalized SDR-to-HDR Conversion with Style Disentangled Representation Learning

Gang He
 Xidian University
 Xi'an, China
 ghe@xidian.edu.cn

Kepeng Xu
 Xidian University
 Xi'an, China
 kepengxu11@gmail.com

Siqi Wang*
 Xidian University
 Xi'an, China
 zgwsq99@163.com

Lin Zhang
 Xidian University
 Xi'an, China
 zlin2309@163.com

Abstract

High-Dynamic-Range Wide-Color-Gamut (HDR-WCG) technology is becoming increasingly prevalent, intensifying the demand for converting Standard Dynamic Range (SDR) content to High Dynamic Range (HDR). Existing methods primarily rely on fixed tone mapping operators, which are inadequate for handling SDR inputs with diverse styles commonly found in real-world scenarios. To address this challenge, we propose a generalized SDR-to-HDR method that tackles diverse styles in real-world SDR content, termed Realistic Style Disentangled Representation Learning (RealRep). By disentangling luminance and chrominance, we analyze the intrinsic differences between contents with varying styles and propose a disentangled multi-view style representation learning method. This approach captures the guidance prior of true luminance and chrominance distributions across different styles, even when the SDR style distributions exhibit significant variations, establishing a robust embedding space for inverse tone mapping. Motivated by the difficulty of directly exploiting degradation representation priors, we propose the Degradation-Domain Aware Controlled Mapping Network (DDACMNet)—a two-stage framework that performs adaptive hierarchical mapping guided by a control-aware normalization mechanism. DDACMNet dynamically modulates the mapping process via degradation-conditioned hierarchical features, enabling robust adaptation across diverse degradation domains. Extensive experiments show that RealRep, consistently outperforms state-of-the-art methods with superior generalization and perceptually faithful HDR color gamut reconstruction.

CCS Concepts

• **Computing methodologies** → **Reconstruction; Computational photography;**

*Corresponding author

Permission to make digital or hard copies of all or part of this work for personal or classroom use is granted without fee provided that copies are not made or distributed for profit or commercial advantage and that copies bear this notice and the full citation on the first page. Copyrights for components of this work owned by others than the author(s) must be honored. Abstracting with credit is permitted. To copy otherwise, or republish, to post on servers or to redistribute to lists, requires prior specific permission and/or a fee. Request permissions from permissions@acm.org.

Conference acronym 'XX, Woodstock, NY

© 2018 Copyright held by the owner/author(s). Publication rights licensed to ACM.

ACM ISBN 978-1-4503-XXXX-X/2018/06

<https://doi.org/XXXXXXX.XXXXXXX>

Keywords

High dynamic range, Wide Color Gamut, inverse tone mapping, Deep learning.

ACM Reference Format:

Gang He, Siqi Wang, Kepeng Xu, and Lin Zhang. 2018. RealRep: Generalized SDR-to-HDR Conversion with Style Disentangled Representation Learning. In *Proceedings of Make sure to enter the correct conference title from your rights confirmation email (Conference acronym 'XX)*. ACM, New York, NY, USA, 10 pages. <https://doi.org/XXXXXXX.XXXXXXX>

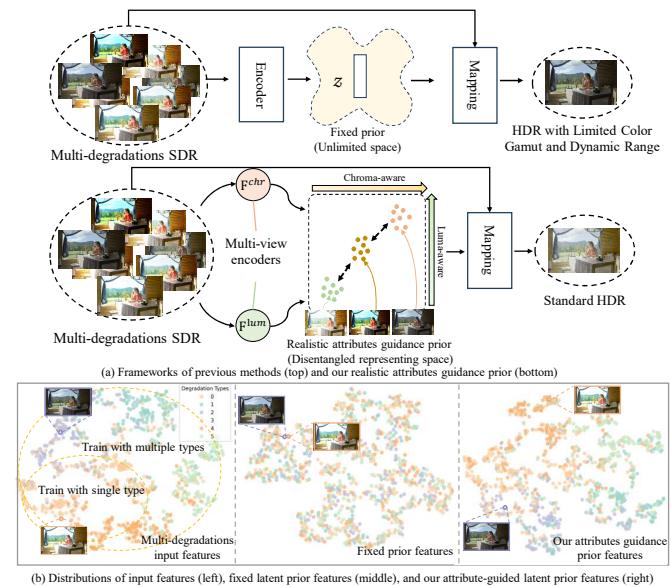


Figure 1: An illustration of our motivation. (a) Comparison between previous frameworks (top) and our realistic attributes guidance prior approach (bottom), where the prior incorporates realistic luminance and chrominance guidance to direct the mapping network. (b) t-SNE visualization of the distributions of SDR input features (left) and latent features (right) after fine-tuning the previous methods' encoder using a multi-degradation dataset.

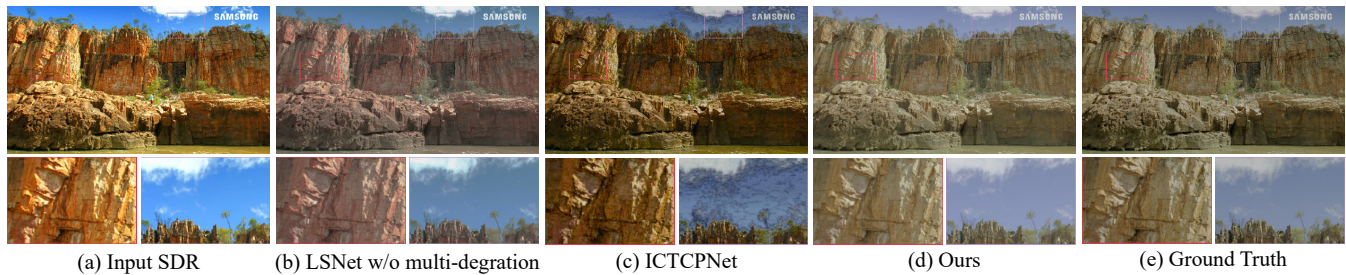


Figure 2: Illustration of the superiority of our approach in recovering luminance and chrominance under unknown degradations. (a) Input SDR image, (b) Results of LSNNet [11] with single degradation training, where the colors closely resemble the input SDR, (c) Results of ICTCPNet [17] with multi-degradation training, which still fail to recover realistic brightness and color, (d) Our proposed method (RealRep) generates the best results, with high-quality recovery in both luminance and chrominance, (e) Ground truth HDR image.

1 Introduction

High Dynamic Range/Wide Color Gamut (HDR/WCG) media, as defined in [33, 35], provides an expanded luminance range and a broader spectrum of visible colors, surpassing the limitations of Standard Dynamic Range (SDR) media. With advancements in display technologies, HDR content has shown significant potential in enhancing visual experiences. In the media and film industries, innovations such as advanced Electro-Optical Transfer Functions (OETFs) like PQ and HLG [19], and Wide Color Gamut (WCG) RGB primaries defined by BT.2020 [18], have further amplified the benefits of HDR. However, the vast majority of existing media content remains in SDR format, restricting its potential on HDR-capable displays. Consequently, Inverse Tone Mapping (iTM), which converts SDR to HDR, has become crucial for leveraging HDR display technology and expanding the usability of SDR content.

Initially, iTM approaches relied on rule-based operations [21–23], enabling limited luminance expansion and color enhancement under specific conditions. However, these methods often suffered from artifacts and poor detail reconstruction, particularly in overexposed or underexposed regions. With the advent of deep learning, learning-based methods have emerged as the dominant approach [7, 11, 34, 38], reframing iTM as a mapping problem between SDR and HDR/WCG. These methods have demonstrated significant advancements in visual quality, addressing limitations of earlier approaches.

In previous approaches, priors have been commonly used to address the ill-posed nature of the inverse tone mapping (iTM) task. These priors were typically predefined, relying on fixed Tone Mapping (TM) operators that perform well under specific conditions but fail to generalize across various types of SDR content. Furthermore, many learning-based methods are implicitly trained on specific tone-mapping operators, which limits their generalization capability. For example, tone-mapping styles tailored for online video platforms such as YouTube often prioritize visual attractiveness, whereas degradation from classical operators like Reinhard aims to preserve the visual dynamic range for content production purposes. Consequently, models trained on a single degradation dataset face inherent limitations in robustness and adaptability. This is illustrated in Figure 1(a), where prior methods employ fixed priors that work when paired with predefined TM operators. However, SDR inputs from different sources exhibit significant variations in

brightness and color levels, leading to substantial discrepancies in the outputs. Even when the encoder is fine-tuned using a multi-degradation dataset, SDR inputs with highly diverse styles tend to cluster into neighboring groups rather than forming well-separated clusters, as shown in Figure 1(b). This suggests that the prior sampling mechanism in earlier methods is unreliable when applied to real-world SDR inputs with varying degradation types.

To address the aforementioned challenges, we propose RealRep, a novel framework for SDR-to-HDR conversion tailored to real-world scenarios involving complex and diverse degradation types. As shown in Figure 4, SDR degradations from different sources exhibit highly varied trends in brightness and chrominance, highlighting the necessity of constructing a robust disentangled representation space that can accurately capture the intrinsic attribute distributions across styles. To this end, RealRep adopts a style-disentangled representation learning strategy that explicitly separates luminance and chrominance features under diverse degradations, enabling the extraction of realistic and generalizable feature-guided representations for inverse tone mapping (iTM). To further improve representation robustness, we introduce the Degradation-Domain Aware Controlled Mapping Network (DDACMNet). DDACMNet is designed to stably leverage the representation priors learned by RealRep, guiding the model to perform consistent and effective mappings under varying degradation conditions. Moreover, by learning from a wide spectrum of degradation types, RealRep significantly expands its learned representation space to encompass a broader and more perceptually accurate color gamut. This allows the framework to model both large-scale luminance variations and fine-grained chromatic structures, enabling reliable luminance expansion and color restoration in highly unconstrained multi-degradation scenarios.

Our main contributions are summarized as follows:

- **Style disentangled representation learning:** We propose RealRep, a novel method that disentangles luminance and chrominance distributions, eliminating the interference caused by differences in diverse styles, and constructs a robust embedding space capable of representing true luminance and chrominance distributions for the SDR-to-HDR task.

- We introduce the Degradation-Domain Aware Controlled Mapping Network (DDACMNet), a dedicated module designed to enhance mapping consistency under varying degradations. By stably leveraging the representation priors learned by RealRep, DDACMNet facilitates dynamic luminance range expansion and color gamut extension through a global-to-local mapping strategy.
- Extensive evaluation on diverse real-world SDR styles: Comprehensive experiments on datasets containing both diverse and unknown SDR styles demonstrate that RealRep consistently outperforms state-of-the-art methods, achieving superior visual quality and strong generalization.

2 Related Work

2.1 Multiple Styles SDR-to-HDR

Although SDR-to-HDR conversion algorithms for media content and consumer-grade displays hold substantial practical value, they have only recently gained attention and emerge. The earliest work in this area, presented by Kim et al. [21], addressed the joint execution of super-resolution (SR) and SDR-to-HDR conversion, utilizing convolutional neural networks (CNNs). Subsequently, Deep SR-ITM [22] introduced a modulation block for spatially adaptive local contrast enhancement. JSI-GAN [23] incorporated pixel-level dynamic convolution for contrast modulation and leveraged generative adversarial networks (GANs) to improve visual quality. Chen et al. [7] proposed the HDRTV1K dataset and HDRTVNet, a network combining adaptive global color mapping, local enhancement, and highlight generation. Xu et al. [38] introduced FMNet, which integrates DCT-based frequency-aware modulation blocks to address artifacts effectively. More recently, Guo et al. [11] proposed the HDRTV4K dataset to address the limitations of existing datasets and introduced LSNet, a luminance segmentation-based solution. They highlighted that existing methods are restricted by their reliance on fixed tone mapping (TM) operators, limiting their ability to generalize across degradations. In this work, we address this limitation through multi-angle representation learning, which extracts generalizable degradation features and enables the network to support multiple SDR-to-HDR mappings without dependence on predefined TM operators.

2.2 Image Enhancement for Multi-Degradations

Image enhancement covers tasks such as super-resolution, denoising, dehazing, deraining, and deblurring. Early deep learning methods typically addressed these tasks separately. For example, SRCNN [8] introduced CNNs for super-resolution, followed by deeper and residual-based architectures [1, 20, 27]. For other tasks, deep models have also shown strong performance in denoising [13, 36, 37], dehazing [25, 40, 41], deraining [15, 26, 39], and deblurring [3, 9, 29]. To overcome the limitations of task-specific models, recent works have proposed unified frameworks for multi-degradation enhancement. IPT [2], AirNet [24], and PromptIR [30] adopt transformers or prompt-guided strategies to handle diverse

degradations within a single model. RAM [31] offers a novel perspective by extracting shared content from degraded images directly, without requiring explicit degradation modeling. These unified methods improve generalization and scalability in real-world scenarios with unknown or mixed degradations.

2.3 Degradation Representation

Degradation representation is critical for guiding effective enhancement, especially under diverse or unknown degradation conditions. Traditional methods often assume known degradation types and estimate parameters, such as noise level in denoising [12, 28] or blur kernel in deblurring [4, 10, 16]. Recent approaches learn implicit representations that encode degradation characteristics without explicit labels. AirNet [24] leverages contrastive learning, while PromptIR [30] conditions restoration with learned prompts. We adopt a similar strategy for multi-style SDR-to-HDR enhancement, learning a degradation-aware representation that captures style-specific information to guide adaptive HDR reconstruction.

3 Methodology

We propose RealRep, a dual-stage framework for SDR-to-HDR restoration, comprising: (1) a representation-learnable multi-view encoder, and (2) a Degradation-Domain Aware Controlled Mapping Network (DDACMNet).

Given an input SDR image x , the encoder extracts hierarchical luminance and chrominance features through two modality-specific branches, yielding e_{lum}^g, e_{lum}^l and e_{chr}^g, e_{chr}^l , where the superscripts g and l denote global and local branches, respectively. These features are supervised via contrastive representation learning, as shown in Fig. 3(b), where global and local projectors generate key-anchor pairs $z_{key}^{g,l}, z_{anchor}^{g,l}$ to ensure semantic consistency across diverse SDR styles. The multi-view encoder outputs are fused using a lightweight Multi-view Fusion Block (f_{fusion} , Fig. 3(c)), producing a unified latent representation z . This representation, along with the input image x , is processed by DDACMNet (f_{DDACM}), which performs progressive SDR-to-HDR mapping under the control of hierarchical degradation priors z_{deg}^g, z_{deg}^l . These priors are extracted from encoder features and injected through controlled affine modulation to enable dynamic, degradation-aware restoration. DDACMNet further enhances spatial details and textures through integrated refinement, yielding high-fidelity HDR reconstruction.

The overall process is formulated as:

$$\hat{y} = f_{DDACM} \left(f_{fusion} \left(e_{lum}^{g,l}, e_{chr}^{g,l} \right), x \right). \quad (1)$$

3.1 Realistic Style Disentangled Representation Learning

3.1.1 Multi-View Representation Extraction. To address the diverse SDR degradations, we design a hierarchical multi-view encoder, based on the autoencoder architecture [32], to extract and normalize luminance and chrominance features, enabling robust SDR-to-HDR conversion. We specifically adopt the UNet architecture as the backbone of our encoder due to its ability to capture both global contextual information and fine-grained local details through its encoder-decoder design and skip connections. As pointed out by [7],

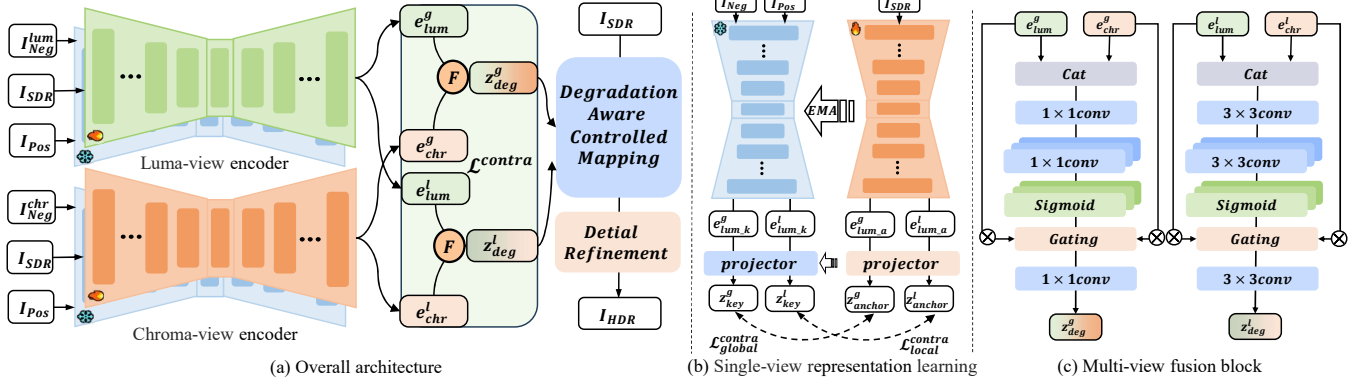


Figure 3: Overview of the proposed multi-degradation SDR-to-HDR framework. The architecture consists of a pair of multi-view degradation encoders that extract global and local representations of luminance and chrominance, a multi-view fusion module that facilitates spatial and channel-wise interaction, and the Degradation-Domain Aware Controlled Mapping Network (DDACMNet) comprising degradation-aware mapping and detail refinement. The encoders are jointly trained with a disentanglement objective to ensure cross-domain consistency. The overall framework enables dynamic luminance expansion and perceptually aligned color gamut reconstruction under diverse degradations.

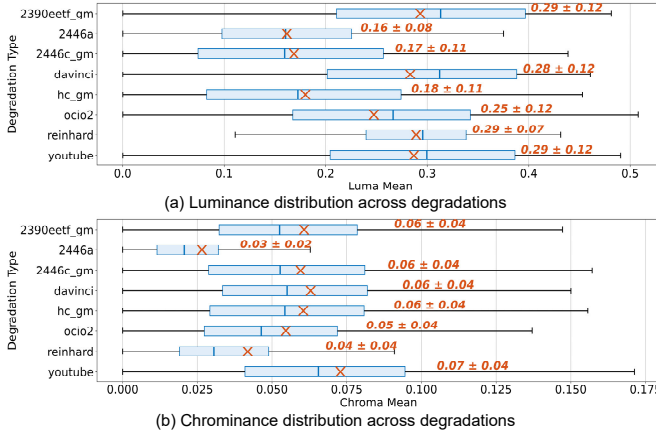


Figure 4: Luminance (a) and chrominance (b) distribution variations across different SDR degradations in the HDRTV4K dataset. Significant distribution differences highlight the need for luminance-chrominance disentangling, enabling more effective representation learning for SDR-to-HDR conversion under diverse degradations.

the SDR/HDR formation process can be effectively modeled as a combination of global and local operators, which aligns well with the inductive bias of UNet. In contrast, we experimented with a ResNet-based encoder and observed that it tends to introduce local structural artifacts and produce suboptimal gamut expansion, particularly in high-saturation regions. These limitations are primarily attributed to its lack of dedicated mechanisms for disentangling and recombining global and spatial context.

The encoder first extracts feature maps e_{lum} and e_{chr} , which capture the luminance and chrominance characteristics of the input x , respectively. These feature maps are then passed through their

corresponding projection heads, ϕ_{lum} and ϕ_{chr} , to obtain normalized global and local representations: z_{lum}^g , z_{chr}^g , z_{lum}^l , and z_{chr}^l . The representation generation is formulated as:

$$z = \frac{\phi(F(x))}{\|\phi(F(x))\|_2}, \quad (2)$$

where $\phi(F(x))$ denotes the transformation of the feature map $F(x)$ via the corresponding projection head.

To learn representations that are aware of both luminance and chrominance modalities, each view-specific encoder F_{lum} and F_{chr} is paired with a structurally identical negative encoder, which encodes negative samples for contrastive learning. Meanwhile, the original feature maps e_{lum} and e_{chr} are preserved for the subsequent SDR-to-HDR transfer stage, as they retain essential spatial and semantic information required for high-quality reconstruction. These features are fed into a multi-view fusion module, which focuses on fusing the luminance and chrominance cues. The fusion process is refined using multi-head convolutions and incorporates a Sigmoid-based gating mechanism to dynamically balance the contributions of each component.

3.1.2 Style Disentangled Representation Learning. The distributions of luminance and chrominance across various SDR degradations exhibit clear inconsistencies, as shown in Figure 4. Such inconsistencies can introduce undesirable interference into the representation space, hindering the model’s ability to learn robust features. To address this issue, we propose a Luma-/Chroma-aware negative exemplar generation strategy. By explicitly separating luminance and chrominance components in the YCbCr color space, this approach eliminates the adverse effects of inconsistent degradation trends and enables independent learning of meaningful features. The detailed procedure of this strategy is illustrated in Algorithm 1. This mechanism ensures the construction of a robust representation space, enhancing the model’s ability to capture true scene characteristics for effective SDR-to-HDR conversion.

Algorithm 1 Luma-/Chroma-aware Negative Exemplars Generation

Input: Multi-degradation dataset D , parameters k_l (luminance negatives), k_c (chrominance negatives)

Output: Luminance negatives N_l , Chrominance negatives N_c

- 1: Initialize $N_l \leftarrow [], N_c \leftarrow []$
- 2: **for** each image $I \in D$ **do**
- 3: Convert to YCbCr: Extract brightness (L_{ref}) and color components (C_{ref})
- 4: Initialize lists $List_l \leftarrow [], List_c \leftarrow []$
- 5: **for** each degradation $x_d \in I$.degradations **do**
- 6: Extract brightness (L_d) and color components (C_d) of x_d
- 7: Compute differences: $D_l \leftarrow \|L_d - L_{\text{ref}}\|_1, D_c \leftarrow \|C_d - C_{\text{ref}}\|_1$
- 8: Append (D_l, x_d) to $List_l$, (D_c, x_d) to $List_c$
- 9: **end for**
- 10: Select top k_l luminance-based and top k_c chrominance-based samples
- 11: $I_l \leftarrow \text{TopK}(List_l, k_l), I_c \leftarrow \text{TopK}(List_c, k_c)$
- 12: **for** each (x_l, x_c) in I_l and I_c **do**
- 13: Add (L_l, C_{ref}) to N_l
- 14: Add (L_{ref}, C_c) to N_c
- 15: **end for**
- 16: **end for**
- 17: Convert N_l, N_c back to RGB
- 18: **Return** N_l, N_c

Positive exemplars are generated by applying random horizontal and vertical flips to the anchor image. This augmentation strategy introduces spatial misalignment while preserving similar brightness and color characteristics, making the resulting samples suitable as positives for contrastive learning. The negative exemplars are designed to emphasize specific differences in brightness and color rather than directly using SDR degradations. Using the L1 norm, the top k luminance-based and chrominance-based samples are selected as negative exemplars. To isolate these differences, additional samples are generated by replacing either the chrominance or luminance channels with those of the anchor. This approach ensures independent brightness and color variations, facilitating robust and disentangled representation learning.

Specifically, the encoder first extracts feature maps e_{lum} and e_{chr} , representing the luminance and chrominance characteristics of the input image I , respectively. These features are then passed through corresponding non-linear projection heads ϕ_{lum} and ϕ_{chr} , designed following the MoCo v2 [5], to obtain the projected representations:

$$z_{\text{lum}} = \phi_{\text{lum}}(e_{\text{lum}}), \quad z_{\text{chr}} = \phi_{\text{chr}}(e_{\text{chr}}). \quad (3)$$

These projected embeddings z_{lum} and z_{chr} serve as the basis for contrastive learning, enabling the model to construct a degradation-invariant and semantically meaningful feature space.

For negative samples $\{N_{\text{lum}}\}$ and $\{N_{\text{chr}}\}$, we define the proposed contrastive learning loss as follows:

$$\mathcal{L}_{\text{contra}} = \sum_{c \in \{\text{lum}, \text{chr}\}} \sum_{s \in \{\text{g}, \text{l}\}} -\log \left(\frac{e^{z_c^s \cdot z_c^{s+}}}{e^{z_c^s \cdot z_c^{s+}} + \sum_{j=1}^{N_c} e^{z_c^s \cdot z_{c,j}^s}} \right) \quad (4)$$

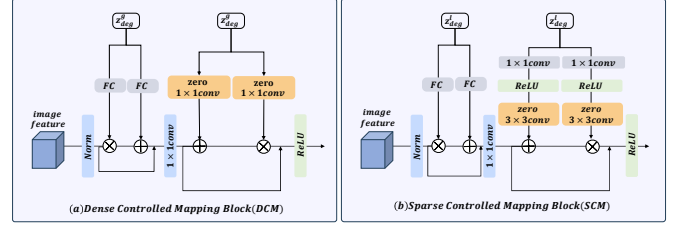


Figure 5: Illustration of (a) Dense Controlled Mapping (DCM) and (b) Sparse Controlled Mapping (SCM).

where $c \in \{\text{lum}, \text{chr}\}$ denotes the feature type, i.e., luminance (lum) or chrominance (chr); $s \in \{\text{g}, \text{l}\}$ denotes the feature scope, i.e., global (g) or local (l); z_c^s is the feature vector of the anchor sample for feature type c and scope s ; z_c^{s+} is the positive sample, which is generated by applying data augmentation to the anchor sample z_c^s ; $z_{c,j}^s$ are negative samples, where $j = 1, 2, \dots, N_c$, and N_c is the total number of negative samples for feature type c .

By pulling the anchor sample and positive sample closer in the representation space while pushing the anchor sample and negative samples apart, the proposed method focuses on learning representations of the inherent luminance and chrominance characteristics of the scene, free from interference by specific styles. This process ensures that the model captures the true priors of luminance and chrominance distributions, effectively disentangling them from the variations introduced by different SDR styles. As a result, the learned representations reflect the underlying real-world luminance and chrominance properties, providing a robust foundation for achieving accurate HDR reconstruction.

3.2 Degradation-Domain Aware Controlled Mapping Network

3.2.1 Degradation-Aware Controlled Mapping. To address complex and spatially diverse degradations in SDR inputs, we introduce two hierarchical modulation modules: Dense Controlled Mapping (DCM) and Sparse Controlled Mapping (SCM). Both perform degradation-aware affine modulation on layer-normalized features, conditioned on global or local degradation priors. To ensure stable learning, we insert a zero-initialized convolution—termed the *control layer*—before injecting priors. Inspired by the soft control mechanism in ControlNet [42], this layer acts as a learnable gate that gradually increases the influence of priors during training.

Directly injecting strong priors (e.g., contrastively pre-trained representations) early in the network often causes misalignment with low-level features, leading to instability. The control layer mitigates this by initially suppressing prior impact, allowing the network to first establish a stable restoration baseline. Over time, it adaptively integrates useful prior cues, improving both training stability and generalization to unseen or compound degradations.

Dense Controlled Mapping (DCM) globally modulates features based on a compact degradation representation. Given a global degradation code $z_{\text{deg}}^g \in \mathbb{R}^{C \times 1 \times 1}$, we use two separate zero-initialized 1×1 convolutions to generate the affine parameters γ and β , i.e., $\gamma = \text{Conv}_\gamma^{1 \times 1}(z_{\text{deg}}^g)$, $\beta = \text{Conv}_\beta^{1 \times 1}(z_{\text{deg}}^g)$. These parameters modulate the normalized input feature via an affine transformation

$\hat{x} = \gamma \cdot x + \beta$. The modulated feature is then refined by a 1×1 convolution and added back to the input through a residual connection. The use of zero-initialized convolutions enables degradation priors to be injected in a stable and learnable manner over the training process. To further enhance normalization under diverse degradations, we extend this design to a degradation-aware Layer Normalization, where the affine parameters γ and β are dynamically generated from z_{deg}^g , allowing the network to adapt its normalization behavior based on the degradation type.

Sparse Controlled Mapping (SCM) handles spatially-varying degradations using a local degradation map $z_{\text{deg}}^l \in \mathbb{R}^{C \times H \times W}$. To generate pixel-wise affine parameters, we apply two parallel branches: each starts with a shared 1×1 convolution followed by ReLU activation, and then a zero-initialized 3×3 convolution to produce either γ or β , i.e., $\gamma = \text{ZeroConv}_{\gamma}^{3 \times 3}(\text{ReLU}(\text{Conv}^{1 \times 1}(z_{\text{deg}}^l)))$, and similarly for β . These parameters are used to modulate the normalized feature spatially as $\hat{x} = \gamma \odot x + \beta$, followed by a 1×1 convolution and residual connection. This design allows fine-grained control of feature adaptation under heterogeneous degradations.

3.2.2 Detail Refinement. Although degradation-aware controlled mapping improves HDR reconstruction, residual discrepancies and high-frequency artifacts may still persist. To address these, we incorporate a Detail Refinement module as the final stage of the DDACMNet. Focused on enhancing texture and detail reconstruction, the refinement module employs Residual Blocks (ResBlocks) and is defined as:

$$F_{\text{refine}}(x) = \text{Conv}_{3 \times 3} \circ [\text{ResBlock}]^{N_r} \circ \text{Conv}_{3 \times 3} \quad (5)$$

$$I_{\text{HDR}} = F_{\text{refine}}(I_{\text{LM}}) \quad (6)$$

where N_r represents the number of stacked ResBlocks. This stage refines the output from the local mapping module (I_{LM}) to produce the final HDR image (I_{HDR}). The DR module ensures high-quality SDR-to-HDR conversion by reconstructing textures and resolving fine details left unaddressed by earlier stages.

3.3 Training Strategy

Our training strategy is tailored for the multi-view degradation encoder and the Degradation-Domain Aware Controlled Mapping network. Inspired by MoCo [14], the encoder is paired with a negative network whose weights are updated using Exponential Moving Average (EMA). This negative encoder helps maintain a slowly evolving representation space, providing stable and consistent targets for contrastive learning. The training process is divided into two stages, with specific adjustments in each stage to optimize learning.

In the first stage, contrastive learning is disabled, and the negative networks in the encoder are frozen to avoid premature noise injection. The control convolutions in the modulation modules are initialized as standard convolutions, and modulation is fully enabled. This allows the encoder and backbone to learn stable feature representations and basic degradation-aware modulation, serving as a strong initialization for the second stage. In the second stage, contrastive learning is introduced to improve the encoder's discrimination of degradation patterns. The control convolutions are re-initialized as zero-initialized layers (ZeroConv), and gradually

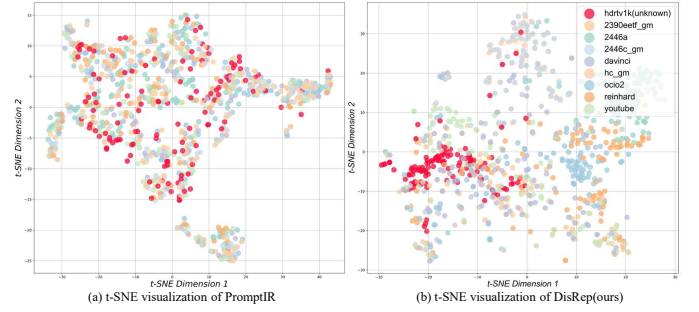


Figure 6: Comparison of t-SNE visualizations for PromptIR (left) and our method (right). Each 2D coordinate represents the projection of a single frame’s feature vector from the corresponding dataset, with PCA (16 components) followed by t-SNE (perplexity=50, n_components=2). The visualizations highlight the structural differences between datasets, with the red points representing features from unknown degradations. This demonstrates our method’s ability to produce a more compact and distinct feature space, as shown by the separation and clustering of both known and unknown degradation types.

trained from zero to softly inject degradation priors. This progressive activation stabilizes the training and prevents disruption from strong contrastive priors, enabling effective adaptation to diverse degradations.

The pixel loss function is defined as:

$$L_{\text{pix}} = \|I_{\text{HDR}}^{\text{pred}} - I_{\text{HDR}}^{\text{G.T.}}\|_1 + \lambda_l \|I_{\text{GM}} - I_{\text{HDR}}^{\text{G.T.}}\|_1, \quad (7)$$

where $I_{\text{HDR}}^{\text{pred}}$ is the predicted HDR image, $I_{\text{HDR}}^{\text{G.T.}}$ is the ground truth HDR image, and λ_l is a hyper-parameter that balances the contributions of the global mapping (GM) loss and the final HDR prediction loss. Here, I_{GM} denotes the intermediate output from the multi-layer DCM module in DDACMNet, which captures the globally modulated representation before detail refinement. Empirically, λ_l is set to 0.7.

The total loss function integrates the pixel loss and contrastive loss as:

$$L_{\text{total}} = L_{\text{pix}} + \lambda_{\text{contra}} L_{\text{contra}} \quad (8)$$

where L_{contra} represents the contrastive loss for robust multi-view representation learning, and λ_{contra} is empirically set to 0.2 to balance the contributions of the two loss terms.

4 Experiments

4.1 Experimental Setup

4.1.1 Dataset. We evaluate the effectiveness of our proposed framework on the HDRTV4K dataset [11], which consists of 3878 4K HDR images encoded in BT.2020/PQ1000. All degradation types included in HDRTV4K are utilized for training and testing. The training set contains 3478 images from HDRTV4K, while the testing set comprises 400 images from HDRTV4K. Additionally, we include 117 images from the HDRTV1K dataset [7] in the testing set to evaluate the performance on unknown degradations, resulting in a total of 517 test images.

Methods	2390eetf_gm	2446a	2446c_gm	davinci	hc_gm	ocio2	reinhard	youtube	Average
	PSNR↑ / SSIM↑								
HDRUNet	29.91 / 0.9219	25.55 / 0.8861	24.17 / 0.8509	23.17 / 0.8790	24.67 / 0.8548	25.12 / 0.8676	23.66 / 0.8887	22.76 / 0.8758	24.88 / 0.8781
HDRTVNet	28.97 / 0.9059	23.73 / 0.8502	26.05 / 0.8597	25.50 / 0.8815	26.91 / 0.8621	26.46 / 0.8699	23.23 / 0.8722	25.31 / 0.8709	25.77 / 0.8716
FMNet	27.96 / 0.9050	23.84 / 0.8753	22.29 / 0.8327	24.48 / 0.8835	23.16 / 0.8390	24.88 / 0.8603	22.26 / 0.8603	24.31 / 0.8755	24.15 / 0.8665
ICTCPNet	29.58 / 0.8548	27.02 / 0.8548	27.76 / 0.8594	25.67 / 0.8705	<u>28.27 / 0.8612</u>	<u>29.97 / 0.8709</u>	25.63 / 0.8694	25.71 / 0.8639	27.45 / 0.8631
LSNet	33.23 / 0.9408	31.18 / 0.9080	28.05 / 0.8731	25.63 / 0.9000	27.34 / 0.8712	29.56 / 0.8913	<u>25.67 / 0.8970</u>	27.01 / 0.9019	28.46 / 0.8979
AirNet	23.00 / 0.8594	21.72 / 0.8519	21.02 / 0.8044	22.22 / 0.8672	21.59 / 0.8107	22.18 / 0.8407	18.72 / 0.8379	22.20 / 0.8512	21.58 / 0.8404
PromptIR	30.06 / 0.9148	30.72 / 0.9073	<u>28.23 / 0.8691</u>	27.83 / 0.9028	28.00 / 0.8740	29.30 / 0.8838	24.97 / 0.8931	27.62 / 0.9068	28.34 / 0.8940
RAM-PromptIR	30.25 / 0.9188	30.83 / 0.9103	28.20 / 0.8711	<u>28.07 / 0.9088</u>	<u>28.09 / 0.8770</u>	29.31 / 0.8828	25.29 / 0.9001	<u>27.77 / 0.9108</u>	<u>28.48 / 0.8975</u>
Ours	34.13 / 0.9507	34.41 / 0.9333	30.38 / 0.8936	30.05 / 0.9266	30.47 / 0.8976	31.36 / 0.9083	27.59 / 0.9292	30.03 / 0.9358	31.05 / 0.9219

Table 1: Comparison of quantitative results on HDRTV4K (known degradation benchmark). All methods were trained using all degraded SDR versions from the HDRTV4K dataset. Bold and underline indicate the best and second-best results, respectively.

Metrics	HDRUNet	HDRTVNet	FMNet	ICTCPNet
PSNR	20.83	<u>23.78</u>	21.61	21.71
SSIM	0.8667	<u>0.8824</u>	0.8609	0.7961
Metrics	LSNet	PromptIR	RAM-PromptIR	Ours
PSNR	20.36	21.24	21.39	29.12
SSIM	0.8603	0.7946	0.8089	0.9412

Table 2: Comparison of quantitative results on HDRTV1K (unknown degradation benchmark). All methods were trained using all degraded SDR versions from the HDRTV4K dataset. Bold and underline indicate the best and second-best results, respectively.

4.1.2 Implementation Details. Each multi-view encoder outputs a global vector and a local feature map with 64 and 16 channels, respectively. The mapping network consists of convolutional layers with 32 channels. We implement our framework using the PyTorch library and adopt the Adam optimizer with $\beta_1 = 0.9$, $\beta_2 = 0.99$, and a learning rate initialized to 2×10^{-4} . The learning rate is scheduled using a MultiStepLR strategy, with decay milestones at 200K and 400K iterations and a decay factor of 0.5. We employ exponential moving average (EMA) with a decay factor of 0.999 to stabilize training. The model is trained for 400K iterations in total, with the first 40K iterations designated as Stage 1. Mixed-precision training with bfloat16 is enabled to improve computational efficiency. We use a mini-batch size of 16, and the training is conducted on an NVIDIA RTX 4090 GPU, taking approximately 3 days to complete.

4.2 Experimental Results

4.2.1 Quantitative Results. We validate RealRep on the HDRTV4K (known degradation benchmark) and HDRTV1K (unknown degradation benchmark) datasets, comparing it to state-of-the-art SDR-to-HDR methods, including HDRUNet[6], HDRTVNet[7], FMNet[38], ICTCPNet[17], LSNet[11], PromptIR[30], and RAM-PromptIR[31].

As shown in Table 1, RealRep outperforms all competing methods on HDRTV4K, demonstrating its ability to handle diverse degradations and produce high-quality HDR reconstructions. This stems from its disentangled multi-view representation learning, which separates luminance and chrominance distributions, enabling robust adaptation to varying degradation characteristics. On HDRTV1K (Table 2), RealRep excels in generalizing to unknown degradations, outperforming methods like HDRUNet, HDRTVNet, and FMNet, which suffer significant performance drops. PromptIR, while effective in simpler tasks like noise removal, struggles

with complex luminance and chrominance transformations. RealRep consistently delivers superior HDR outputs, leveraging its disentangled encoder and domain-adaptive transfer framework.

4.2.2 Qualitative Results. Figure 7 compares HDR/WCG images generated by state-of-the-art methods and our proposed RealRep framework. Existing methods, such as HDRTVNet, FMNet, and ICTCPNet, struggle with diverse degradations, causing artifacts like banding, color distortion, and uneven luminance due to their reliance on fixed tone mapping strategies, which limits adaptability and leads to inconsistent performance. For instance, HDRTVNet produces overexposure and banding, FMNet shows luminance and chrominance mismatches, and ICTCPNet renders desaturated colors. In contrast, RealRep combines disentangled multi-view degradation representation learning with a domain-adaptive hierarchical transfer framework to dynamically adapt to varying degradations, producing HDR images that are natural, consistent, and artifact-free. These qualities are evident in Figure 6, where RealRep achieves smoother luminance transitions, better highlight recovery, and accurate color distributions, surpassing other methods in addressing unknown degradations and delivering results closer to the ground truth.

4.2.3 Joint Luma-/Chroma-aware Representation Visualization. To demonstrate the effectiveness of RealRep in constructing the inverse tone mapping (iTm) embedding space and its generalization to unknown degradations, we performed t-SNE visualization of the feature space. As shown in Figure 3, the left panel depicts the prompt representations extracted by PromptIR, while the right panel illustrates the degradation features extracted by RealRep. In PromptIR’s feature space, unknown degradations (e.g., HDRTV1K) are scattered and overlap with other clusters, indicating poor generalization to unseen scenarios. In contrast, RealRep produces compact and well-separated clusters for HDRTV1K, showcasing superior generalization to unknown degradations and a more structured feature space. These findings highlight the strength of RealRep in addressing diverse real-world degradations.

4.3 Ablation Studies.

In this section, we conduct a series of ablation experiments to investigate the effectiveness of the decoupled multi-view representations and degradation-aware controlled mapping module.

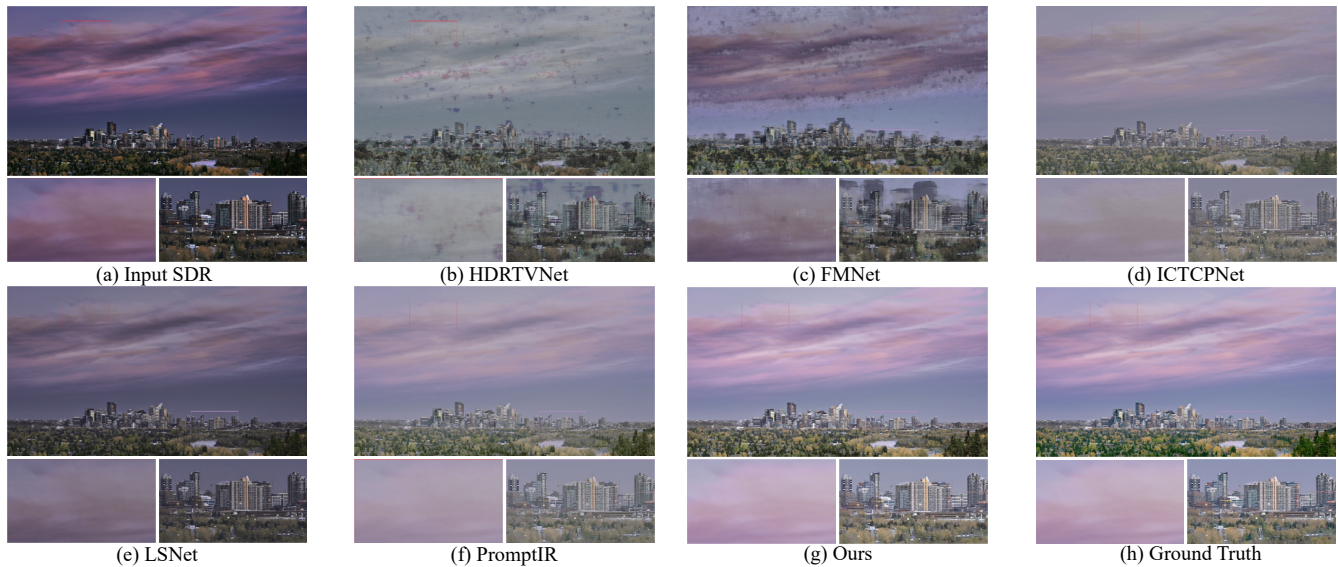


Figure 7: Visual comparison with the state-of-the-art methods. Following hdrtdm [11], the HDR images are shown in their original encoding without tone mapping to preserve highlights. Transfer function and gamut mismatches may cause darker, less saturated grayish appearance on paper or SDR screens.

Configuration	2390eetf_gm	2446a	2446c_gm	davinci	Avg.
Baseline	27.37	27.72	25.96	25.67	25.74
RealRep w/o fusion	32.27	32.76	29.68	27.71	29.83
RealRep w/o z_{lum}	32.96	27.88	27.53	29.37	28.96
RealRep w/o z_{chr}	32.92	29.48	28.40	29.42	29.58
RealRep w/o \mathcal{L}_{contra}	33.73	29.71	28.23	29.77	30.04
RealRep	34.29	34.83	31.10	30.17	31.42

Table 3: Ablation on multi-view representations and multi-view fusion, evaluated by PSNR (dB). The final column reports the average across all eight degradation types. Due to space limitations, only four representative degradations are shown.

Configuration	2390eetf_gm	2446a	2446c_gm	davinci	hdrtv1k	Avg.
RealRep w/o z_{global}	24.56	23.43	28.41	22.41	25.03	25.00
RealRep w/o z_{local}	32.95	34.00	30.90	27.33	28.42	30.28
RealRep w/o control	33.24	33.55	30.35	29.49	28.37	30.47
RealRep	34.29	34.83	31.10	30.17	29.12	31.16

Table 4: Ablation on the degradation-aware controlled mapping module, evaluated by PSNR (dB).

4.3.1 Ablation of Disentangled Multi-View Representations. To evaluate the effectiveness of disentangled multi-view representations, we conduct ablation experiments on the luminance representation z_{lum} , chrominance representation z_{chr} , their combination, the contrastive loss \mathcal{L}_{contra} , and the multi-view fusion module. As shown in Table 3, the baseline model, which lacks all multi-view representations and fusion, achieves the lowest average PSNR of 25.74dB, highlighting the necessity of these components. Removing either z_{lum} or z_{chr} reduces the average PSNR to 28.96dB and 29.58dB, respectively, underscoring their independent contributions. The absence of the multi-view fusion module, which integrates luminance and chrominance features, further lowers the average PSNR

to 29.83dB, demonstrating its importance for balancing and integrating these representations. Furthermore, removing the contrastive loss \mathcal{L}_{contra} leads to a performance drop from 31.42dB to 30.04dB, suggesting that the contrastive learning space plays a crucial role in guiding the model to extract informative and discriminative priors. The full RealRep model achieves the highest average PSNR of 31.42dB, validating the joint effectiveness of multi-view representations, fusion, and contrastive supervision in enhancing SDR-to-HDR performance.

4.3.2 Ablation of Degradation-Domain Aware Controlled Mapping Network. We further investigate the impact of the degradation-aware controlled module by conducting ablation experiments on its global and local mapping components, as well as the control mechanism. As shown in Table 4, removing either the global mapping or local mapping leads to a noticeable performance drop, with average PSNRs of 25.00dB and 30.28dB, respectively, validating their complementary roles in capturing hierarchical domain knowledge. Notably, the control mechanism—comprising a zero-initialized convolution and a two-stage training strategy—plays a key role in enhancing generalization. Removing it leads to a decline in both overall performance and generalization ability, with the average PSNR dropping from 31.16dB to 30.78dB, and the PSNR on the challenging HDRTV1K dataset decreasing from 29.12dB to 28.87dB. These results highlight the effectiveness of the control design in improving transferability and robustness across diverse and unseen degradation scenarios. The full RealRep model consistently achieves the best results, demonstrating the importance of the complete degradation-aware controlled mapping design.

4.3.3 Ablation of encoder architecture. We compare ResNet and our UNet-based encoder under identical training settings (batch size = 16, 100K iterations). As shown in Table 5, the UNet encoder

achieves better performance (27.28 dB vs. 26.87 dB) with fewer parameters (0.50M vs. 1.23M), demonstrating its superior efficiency and representation capability.

Encoder	Parameters (M)	PSNR (dB)
ResNet Encoder	1.2289	26.87
UNet Encoder (Ours)	0.5044	27.28

Table 5: Ablation on encoder architecture. UNet-based encoder outperforms ResNet under identical training settings.

5 Concluding Remarks

This paper presents RealRep, a novel SDR-to-HDR method designed for real-world scenarios with diverse SDR styles. RealRep tackles luminance and chrominance variations using style disentangled representation learning, capturing intrinsic style differences to provide realistic guidance for inverse tone mapping. A Degradation-Domain Aware Controlled Mapping framework further enables dynamic luminance range expansion and color gamut extension. Evaluations on diverse and unknown degradations demonstrate our superiority over state-of-the-art methods in visual quality and generalization. Future work will explore extending RealRep to video HDR conversion and real-time applications.

References

- [1] Namhyuk Ahn, Byungkon Kang, and Kyung-Ah Sohn. 2018. *Fast, Accurate, and Lightweight Super-Resolution with Cascading Residual Network*. 256–272. doi:10.1007/978-3-030-01249-6_16
- [2] Hanting Chen, Yunhe Wang, Tianyu Guo, Chang Xu, Yiping Deng, Zhenhua Liu, Siwei Ma, Chunjing Xu, Chao Xu, and Wen Gao. 2021. Pre-Trained Image Processing Transformer. In *2021 IEEE/CVF Conference on Computer Vision and Pattern Recognition (CVPR)*. doi:10.1109/cvpr46437.2021.01212
- [3] Liang Chen, Faming Fang, Shen Lei, Fang Li, and Guixu Zhang. 2020. *Enhanced Sparse Model for Blind Deblurring*. 631–646. doi:10.1007/978-3-030-58595-2_38
- [4] Liang Chen, Jiawei Zhang, Songnan Lin, Faming Fang, and Jimmy S. J. Ren. 2021. Blind Deblurring for Saturated Images. *2021 IEEE/CVF Conference on Computer Vision and Pattern Recognition (CVPR) (2021)*, 6304–6312. <https://api.semanticscholar.org/CorpusID:235656945>
- [5] Xinlei Chen, Haoqi Fan, Ross B. Girshick, and Kaiming He. 2020. Improved Baselines with Momentum Contrastive Learning. *ArXiv abs/2003.04297 (2020)*. <https://api.semanticscholar.org/CorpusID:212633993>
- [6] Xiangyu Chen, Yihao Liu, Zhengwen Zhang, Y. Qiao, and Chao Dong. 2021. HDRUNet: Single Image HDR Reconstruction with Denoising and Dequantization. *2021 IEEE/CVF Conference on Computer Vision and Pattern Recognition Workshops (CVPRW) (2021)*, 354–363. <https://api.semanticscholar.org/CorpusID:235212387>
- [7] Xiangyu Chen, Zhengwen Zhang, Jimmy S. J. Ren, Lynhoo Tian, Y. Qiao, and Chao Dong. 2021. A New Journey from SDRTV to HDRTV. *2021 IEEE/CVF International Conference on Computer Vision (ICCV) (2021)*, 4480–4489. <https://api.semanticscholar.org/CorpusID:237194979>
- [8] Chao Dong, Chen Change Loy, Kaiming He, and Xiaoou Tang. 2014. *Learning a Deep Convolutional Network for Image Super-Resolution*. 184–199. doi:10.1007/978-3-319-10593-2_13
- [9] Thomas Eboli, Jian Sun, and Jean Ponce. 2020. End-to-end Interpretable Learning of Non-blind Image Deblurring. *Le Centre pour la Communication Scientifique Directe - HAL - Diderot, Le Centre pour la Communication Scientifique Directe - HAL - Diderot (Aug 2020)*.
- [10] Dong Gong, Jie Yang, Lingqiao Liu, Yanning Zhang, Ian D. Reid, Chunhua Shen, Anton van den Hengel, and Javen Qinfeng Shi. 2016. From Motion Blur to Motion Flow: A Deep Learning Solution for Removing Heterogeneous Motion Blur. *2017 IEEE Conference on Computer Vision and Pattern Recognition (CVPR) (2016)*, 3806–3815. <https://api.semanticscholar.org/CorpusID:18123440>
- [11] Cheng Guo, Leidong Fan, Ziyu Xue, and Xiuhua Jiang. 2023. Learning a Practical SDR-to-HDRTV Up-conversion using New Dataset and Degradation Models. In *2023 IEEE/CVF Conference on Computer Vision and Pattern Recognition (CVPR)*. 22231–22241. doi:10.1109/CVPR52729.2023.02129
- [12] Shi Guo, Zifei Yan, K. Zhang, Wangmeng Zuo, and Lei Zhang. 2018. Toward Convolutional Blind Denoising of Real Photographs. *2018 IEEE/CVF Conference on Computer Vision and Pattern Recognition (CVPR) (2018)*, 1712–1722. <https://api.semanticscholar.org/CorpusID:49672261>
- [13] Shi Guo, Zifei Yan, Kai Zhang, Wangmeng Zuo, and Lei Zhang. 2019. Toward Convolutional Blind Denoising of Real Photographs. In *2019 IEEE/CVF Conference on Computer Vision and Pattern Recognition (CVPR)*. doi:10.1109/cvpr.2019.00181
- [14] Kaiming He, Haoqi Fan, Yuxin Wu, Saining Xie, and Ross B. Girshick. 2019. Momentum Contrast for Unsupervised Visual Representation Learning. *2020 IEEE/CVF Conference on Computer Vision and Pattern Recognition (CVPR) (2019)*, 9726–9735. <https://api.semanticscholar.org/CorpusID:207930212>
- [15] Xiaowei Hu, Chi-Wing Fu, Lei Zhu, and Pheng-Ann Heng. 2019. Depth-Attentional Features for Single-Image Rain Removal. In *2019 IEEE/CVF Conference on Computer Vision and Pattern Recognition (CVPR)*. doi:10.1109/cvpr.2019.00821
- [16] Zhe Hu, Sunghyun Cho, Jue Wang, and Ming-Hsuan Yang. 2014. Deblurring Low-Light Images with Light Streaks. *2014 IEEE Conference on Computer Vision and Pattern Recognition (2014)*, 3382–3389. <https://api.semanticscholar.org/CorpusID:10184760>
- [17] Peihuan Huang, Gaofeng Cao, Fei Zhou, and Guoping Qiu. 2023. Video Inverse Tone Mapping Network with Luma and Chroma Mapping. *Proceedings of the 31st ACM International Conference on Multimedia (2023)*. <https://api.semanticscholar.org/CorpusID:264492628>
- [18] International Telecommunication Union (ITU). 2015. *Parameter Values for Ultra-High Definition Television Systems for Production and International Programme Exchange (2 ed.)*. Technical Report ITU-R BT.2020-2. International Telecommunication Union, Geneva, Switzerland. 1–2 pages.
- [19] International Telecommunication Union (ITU). 2018. *Image Parameter Values for High Dynamic Range Television for Use in Production and International Programme Exchange (2 ed.)*. Technical Report ITU-R BT.2100-2. International Telecommunication Union, Geneva, Switzerland. 1–2 pages.
- [20] Jiwon Kim, Jung Kwon Lee, and Kyoung Mu Lee. 2016. Accurate Image Super-Resolution Using Very Deep Convolutional Networks. In *2016 IEEE Conference on Computer Vision and Pattern Recognition (CVPR)*. doi:10.1109/cvpr.2016.182
- [21] Soo Ye Kim and Munchurl Kim. 2018. A Multi-purpose Convolutional Neural Network for Simultaneous Super-Resolution and High Dynamic Range Image Reconstruction. In *Asian Conference on Computer Vision*. <https://api.semanticscholar.org/CorpusID:168633755>
- [22] Soo Ye Kim, Jihyong Oh, and Munchurl Kim. 2019. Deep SR-ITM: Joint Learning of Super-Resolution and Inverse Tone-Mapping for 4K UHD HDR Applications. *2019 IEEE/CVF International Conference on Computer Vision (ICCV) (2019)*, 3116–3125. <https://api.semanticscholar.org/CorpusID:131779280>
- [23] Soo Ye Kim, Jihyong Oh, and Munchurl Kim. 2019. JSI-GAN: GAN-Based Joint Super-Resolution and Inverse Tone-Mapping with Pixel-Wise Task-Specific Filters for UHD HDR Video. In *AAAI Conference on Artificial Intelligence*. <https://api.semanticscholar.org/CorpusID:202542696>
- [24] Boyun Li, Xiao Liu, Peng Hu, Zhongqin Wu, Jiancheng Lv, and Xiaocui Peng. 2022. All-In-One Image Restoration for Unknown Corruption. *2022 IEEE/CVF Conference on Computer Vision and Pattern Recognition (CVPR) (2022)*, 17431–17441. <https://api.semanticscholar.org/CorpusID:250551851>
- [25] Boyi Li, Xiulian Peng, Zhangyang Wang, Jizheng Xu, and Dan Feng. 2017. An All-in-One Network for Dehazing and Beyond. *Cornell University - arXiv, Cornell University - arXiv (Jul 2017)*.
- [26] Siyuan Li, Wenqi Ren, Feng Wang, Iago Breno Araujo, Eric K. Tokuda, Roberto Hirata Junior, Roberto M. Cesar, Zhangyang Wang, and Xiaochun Cao. 2021. A Comprehensive Benchmark Analysis of Single Image Deraining: Current Challenges and Future Perspectives. *International Journal of Computer Vision (Apr 2021)*, 1301–1322. doi:10.1007/s11263-020-01416-w
- [27] Bee Lim, Sanghyun Son, Heewon Kim, Seungjun Nah, and Kyoung Mu Lee. 2017. Enhanced Deep Residual Networks for Single Image Super-Resolution. In *2017 IEEE Conference on Computer Vision and Pattern Recognition Workshops (CVPRW)*. doi:10.1109/cvprw.2017.151
- [28] Xinhao Liu, Masayuki Tanaka, and M. Okutomi. 2013. Single-Image Noise Level Estimation for Blind Denoising. *IEEE Transactions on Image Processing* 22 (2013), 5226–5237. <https://api.semanticscholar.org/CorpusID:15941714>
- [29] Bao-Liang Lu, Jun-Cheng Chen, and Rama Chellappa. 2019. Unsupervised Domain-Specific Deblurring via Disentangled Representations. *Cornell University - arXiv, Cornell University - arXiv (Mar 2019)*.
- [30] Vaishnav Potlapalli, Syed Waqas Zamir, Salman Siddique Khan, and Fahad Shahbaz Khan. 2023. PromptIR: Prompting for All-in-One Blind Image Restoration. *ArXiv abs/2306.13090 (2023)*. <https://api.semanticscholar.org/CorpusID:259224666>
- [31] Chuntao Qin, Ruiqi Wu, Zikun Liu, Xin Lin, Chun-Le Guo, Hyun Hee Park, and Chongyi Li. 2024. Restore Anything with Masks: Leveraging Mask Image Modeling for Blind All-in-One Image Restoration. In *European Conference on Computer Vision*. <https://api.semanticscholar.org/CorpusID:272987034>
- [32] Olaf Ronneberger, Philipp Fischer, and Thomas Brox. 2015. U-Net: Convolutional Networks for Biomedical Image Segmentation. *ArXiv abs/1505.04597 (2015)*. <https://api.semanticscholar.org/CorpusID:3719281>
- [33] BT Series. 2012. *Parameter values for ultra-high definition television systems for production and international programme exchange*. Technical Report BT.2020. International Telecommunication Union - Telecommunication Standardization Sector (ITU-T). 1–7 pages.

- [34] Tong Shao, Deming Zhai, Junjun Jiang, and Xianming Liu. 2022. Hybrid Conditional Deep Inverse Tone Mapping. *Proceedings of the 30th ACM International Conference on Multimedia* (2022). <https://api.semanticscholar.org/CorpusID:252782392>
- [35] SMPTE Standard. 2014. *High dynamic range electro-optical transfer function of mastering reference displays*. Technical Report ST 2084. Society of Motion Picture and Television Engineers (SMPTE). 11 pages.
- [36] Chunwei Tian, Yong Xu, Zuoyong Li, Wangmeng Zuo, Lunke Fei, and Hong Liu. 2020. Attention-guided CNN for image denoising. *Neural Networks* (Apr 2020), 117–129. doi:10.1016/j.neunet.2019.12.024
- [37] Jia Xixi, Sanyang Liu, Xiaoyi Feng, and Lei Zhang. 2019. FOCNet: A Fractional Optimal Control Network for Image Denoising. *IEEE Conference Proceedings, IEEE Conference Proceedings* (Jan 2019).
- [38] Gang Xu, Qibin Hou, Le Zhang, and Ming-Ming Cheng. 2022. FMNet: Frequency-Aware Modulation Network for SDR-to-HDR Translation. *Proceedings of the 30th ACM International Conference on Multimedia* (2022). <https://api.semanticscholar.org/CorpusID:252783139>
- [39] Wenhan Yang, Jiaying Liu, Shuai Yang, and Zongming Guo. 2019. Scale-Free Single Image Deraining Via Visibility-Enhanced Recurrent Wavelet Learning. *IEEE Transactions on Image Processing* (Jun 2019), 2948–2961. doi:10.1109/tip.2019.2892685
- [40] Xitong Yang, Zheng Xu, and Jiebo Luo. 2022. Towards Perceptual Image Dehazing by Physics-Based Disentanglement and Adversarial Training. *Proceedings of the AAAI Conference on Artificial Intelligence* (Jun 2022). doi:10.1609/aaai.v32i1.12317
- [41] He Zhang and VishalM. Patel. 2018. Densely Connected Pyramid Dehazing Network. *Cornell University - arXiv, Cornell University - arXiv* (Mar 2018).
- [42] Lvmin Zhang, Anyi Rao, and Maneesh Agrawala. 2023. Adding Conditional Control to Text-to-Image Diffusion Models. *2023 IEEE/CVF International Conference on Computer Vision (ICCV)* (2023), 3813–3824. <https://api.semanticscholar.org/CorpusID:256827727>